




First-Principles Study of Structural, Elastic, and Thermodynamic Properties of PdSn₄ with Ni Addition

YALI TIAN ^{1,3} LIFANG ZHANG,¹ and PING WU^{2,4}

1.—Department of Applied Physics, Tianjin University of Commerce, Tianjin 300134, People's Republic of China. 2.—Department of Applied Physics, Institute of Advanced Materials Physics, Tianjin Key Laboratory of Low Dimensional Materials Physics and Preparing Technology, Faculty of Science, Tianjin University, Tianjin 300072, People's Republic of China. 3.—e-mail: lxytyl@tjcu.edu.cn. 4.—e-mail: pingwu@tju.edu.cn

The structural, mechanical, thermodynamic, and electronic properties of PdSn₄ with Ni addition are investigated by first-principles calculations. Substitution of Ni for Pd in PdSn₄ causes a decrease of the lattice constants as well as cell volume due to the smaller atomic radius of Ni compared with Pd. The studied structures are thermodynamically stable, but the stability decreases with increasing Ni concentration. The bulk modulus increases while the shear modulus, Young's modulus, hardness, Debye temperature, and minimum heat transfer ability decrease on Ni substitution. PdSn₄ is elastic–brittle. Substitution leads to a ductile structure, and the ductility increases with the Ni fraction except for Pd₂Ni₂Sn₁₆. The anisotropic character is estimated both based on the formula and graphically, revealing an increasing anisotropic tendency after substitution. Based on their total density of states, all the compounds are metallic. Substitution decreases the hybridization of Pd-*d* and Sn-*p* states in the lower energy range but increases the hybridization of Ni-*d* and Sn-*p* electrons near the Fermi level.

Key words: First-principles calculations, intermetallic compounds, mechanical properties, brittleness and ductility

INTRODUCTION

In the field of electronic packaging, trilayer Au/Pd/Ni(P) surface finishes offer low cost and high reliability when used in wire-bonding and soldering applications.^{1,2} In such systems, a Pd layer, often with thickness of 0.2 μm, is electroless deposited between a thinner layer of about 0.1 μm of Au and a thicker layer of 7 μm of Ni(P) to improve the wettability.^{3,4} The upper Au layer serves as an effective oxidation resistance layer. The central Pd layer can not only improve the wettability but also protect the Ni(P) layer against corrosion, since hypercorrosion of the Ni(P) layer could reduce the wettability between the solder and substrate, degrading the interfacial strength. Meanwhile, the

Ni(P) underlayer plays the role of a diffusion barrier to prevent the rapid reaction between Sn in the main body of the lead-free solder with the Cu substrate. During soldering, Au atoms may diffuse into the solder matrix, forming Au–Sn intermetallics such as AuSn₄ and possibly AuSn₂.⁴ With the exhaustion of the Au layer at the interface, the Pd layer will become exposed to solder and react with the contained Sn to form Pd–Sn intermetallics. According to literature, PdSn₄ exhibits a high growth rate in Sn-based or Sn–Ag–Cu solder joints on Pd substrates, and its growth may proceed by not only solid- but also liquid-state reaction.⁵ At the interface between the solder and Ni substrate, Ni atoms may diffuse into the structure of PdSn₄ to form (Pd,Ni)Sn₄ phase, effectively retarding the electromigration damage. Recent studies have shown that the electromigration resistance of (Pd,Ni)Sn₄ is closely related to the Ni content.⁶ To be specific, if the solubility of Ni reaches 17 at.%,

(Received March 27, 2019; accepted November 12, 2019; published online November 26, 2019)

the (Pd,Ni)Sn₄ layer cannot retard electromigration, while (Pd,Ni)Sn₄ with Ni content below 3 at.% can offer effective electromigration resistance. Based on the Pd–Ni–Sn ternary phase diagram, PdSn₄ has high solubility for Ni atoms,⁷ resulting in a structure that is usually denoted as (Pd,Ni)Sn₄.^{8,9} Kajihara et al. reported that Ni atoms can dissolve in PdSn₄ up to 17.6 at.% in the Sn-4.5 wt.%Pd/Ni system at 200°C.⁹ In fact, the Ni content in PdSn₄ may vary between samples, depending on the specific reaction condition. Ho et al. found that a phase with composition (Pd_{0.26}Ni_{0.74})Sn₄ appeared at the Sn-0.1 wt.%Pd/Ni₃Sn₄ interface.⁷ With the help of (Pd,Ni)Sn₄, interconnections between the solder matrix and Ni substrate can be effectively realized.

As mentioned above, PdSn₄ intermetallics have been widely reported in many works. However, most of them focused on the interfacial reaction products, whereas the intrinsic features including the bulk modulus, shear modulus, thermodynamic and electronic properties of PdSn₄ remain unknown, in particular when Ni is substituted in this phase. To complete the database of physical properties for PdSn₄-based intermetallics, further studies are thus necessary. In the work presented herein, a first-principles study on PdSn₄-based intermetallics is carried out to predict their intrinsic structural, mechanical, thermodynamic, and electronic properties. These findings will help to reveal the structural stability and mechanical properties of these intermetallics.

CALCULATION PROCEDURES

The crystal structure of PdSn₄, which resembles that of AuSn₄ and PtSn₄, belongs to the orthorhombic crystal system with lattice constants $a = 6.38881 \text{ \AA}$, $b = 6.44151 \text{ \AA}$, and $c = 11.44622 \text{ \AA}$ in space group no. 41 with symmetry type Aba2 and Pearson symbol *oC20*.¹⁰ The lattice structure is shown in Fig. 1 together with four equivalent Pd sites labeled with Arabic numerals. Due to the fact that Ni atoms can substitute at Pd sites in PdSn₄ lattice, it is reasonable to believe that (Pd,Ni)Sn₄ will have the same crystal structure as PdSn₄. Altogether, the PdSn₄ lattice contains 20 atoms, viz. 4 Pd and 16 Sn atoms. Therefore, PdSn₄ should in fact be expressed as Pd₄Sn₁₆. If one Pd atom in the PdSn₄ lattice is replaced by Ni, the stoichiometric ratio thus becomes Pd₃NiSn₁₆ (namely Pd_{0.75}Ni_{0.25}Sn₄, corresponding to 5 at.% Ni solubility in the PdSn₄ lattice). When two Pd atoms are replaced by Ni, the formula becomes Pd₂Ni₂Sn₁₆ (namely Pd_{0.5}Ni_{0.5}Sn₄, corresponding to 10 at.% Ni solubility in PdSn₄). Similarly, the lattice will be PdNi₃Sn₁₆ (namely Pd_{0.25}Ni_{0.75}Sn₄, corresponding to 15 at.% Ni solubility in PdSn₄) if three Pd atoms are replaced by Ni. Due to the high solubility of Ni in PdSn₄, we also make a bold attempt to substitute Ni at all the Pd sites, resulting in NiSn₄. Literature

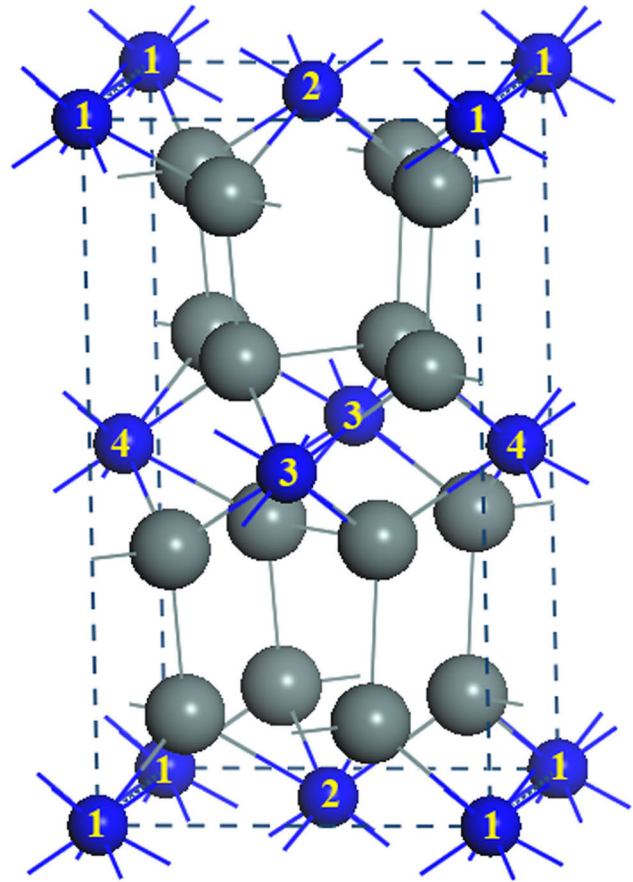


Fig. 1. Crystal structure of PdSn₄ (tin atoms are big and grey, palladium atoms are small and blue) (Color figure online).

review reveals that NiSn₄ could be grown by solidification of Sn–Ni alloys containing 0 wt.% to 0.45 wt.% Ni in Belyakov's work,¹¹ and also using different types of Sn/Ni diffusion couple in Leinewebner's study.¹² The structure was analyzed by Boettinger et al. using electron backscatter diffraction analysis, revealing it to be of PtSn₄ type with Aba2 symmetry.¹³ Therefore, in the present work, first-principles calculations are carried out for Pd_{1-x}Ni_xSn₄ ($x = 0, 0.25, 0.5, 0.75, 1$) materials to predict their possible properties. The different concentrations of Ni substitution in the structures are achieved by interchanging the possible positions of different Pd sites in the PdSn₄ lattice as shown in Fig. 1; For example, four different configurations are possible for Pd₃NiSn₁₆, since the Ni atom can occupy the Pd sites labeled 1, 2, 3, or 4, as illustrated in Fig. 1. For Pd₂Ni₂Sn₁₆, six different configurations can be formed, because Ni atoms can occupy the Pd sites labeled 1 + 2, 1 + 3, 1 + 4, 2 + 3, 2 + 4, and 3 + 4. For PdNi₃Sn₁₆, four configurations can be achieved by substituting at the Pd sites labeled 1 + 2 + 3, 1 + 2 + 4, 2 + 3 + 4, and 1 + 3 + 4. To detect which of these is the ground state, all of the configurations should be computed.

First-principles calculations are performed using the Vienna *ab initio* simulation package (VASP)

code¹⁴ with the generalized gradient approximation (GGA) of Perdew–Burke–Ernzerhof (PBE)¹⁵ to treat the exchange–correlation function. The integration in the Brillouin zone is carried out using $6 \times 6 \times 4$ Monkhorst–Pack¹⁶ **k**-grid meshes. The electronic partial occupancies are set using the Methfessel–Paxton scheme with 0.1 eV smearing.¹⁷ The cutoff energy is chosen as 450 eV after a convergence test for PdSn₄ with a convergence threshold on the total energy of less than 1×10^{-5} eV/atom. The valence electron configurations are taken as $3d^8 4s^2$ for Ni, $5s^2 5p^2$ for Sn, and $4d^{10}$ for Pd. During the structure optimization, the volume and cell are allowed to change. After that, a static total energy calculation is carried out to obtain the total energy of the crystal system.

RESULTS AND DISCUSSION

Structure and Phase Stability

According to the reported structure of PdSn₄, the lattice parameters and inner atomic positions of PdSn₄ are first optimized; the results are listed in Table I, revealing that the derived lattice constants are larger than the original values¹⁰ by less than 2.4%. This difference lies in the expected range, since the GGA method often overestimates the lattice parameters. This finding confirms that the method applied herein is suitable and that the derived results are reliable. For the Ni-substituted intermetallics, the lattice constants and volumes are all smaller than those of the parent PdSn₄ material, due to the smaller atomic radius of Ni compared with Pd. To estimate the stability of the Ni-substituted PdSn₄ structures, the energy of formation ΔH was calculated using the formula¹⁸

$$\Delta H = \frac{1}{5} [E_{\text{Pd}_{1-x}\text{Ni}_x\text{Sn}_4} - ((1-x)E_{\text{Pd}} + xE_{\text{Ni}} + 4E_{\text{Sn}})]. \quad (1)$$

Here, $E_{\text{Pd}_{1-x}\text{Ni}_x\text{Sn}_4}$ is the total energy of Pd_{1-x}Ni_xSn₄ in the relaxed state and E_{Pd} , E_{Ni} , and E_{Sn} are the per atomic energy of face-centered cubic (fcc) Pd, fcc Ni, and β -Sn in solid state. A negative energy of formation implies a thermodynamically stable structure. Moreover, the more negative the energy of formation, the more stable the compound. The energies of formation calculated for Pd_{1-x}Ni_xSn₄ are also presented in Table I. For pure PdSn₄, the calculated energy of formation is -26.35 kJ/mol atom, very close to the *ab initio* value of -0.307 eV/atom (corresponding to -29.61 kJ/mol atom) reported in Ref. 19. Note that the crystal structure of the PdSn₄ prepared by powder refinement in Ref. 19 was centrosymmetric in space group *Ccca* (no. 68) with lattice parameters $a = 6.4421$ Å, $b = 11.4451$ Å, and $c = 6.3891$ Å. Although the crystal structure in the cited work is different from that considered herein, the energy of formation may still characterize the stability of the compound when Pd and Sn form PdSn₄. To determine the exact ground state for the Ni-substituted phases with given concentration, the lowest energy of formation is used as a criterion. To be specific, the energy of formation is lowest for Pd₃NiSn₁₆ with the Ni atom at Pd site 3. For Ni₂Pd₂Sn₁₆, the Ni atoms preferential occupy Pd sites 2 + 3 rather than the other combinations due to its lower energy of formation. For Ni₃PdSn₁₆, the Ni atoms are most likely to occupy Pd sites 2 + 3 + 4, although the energies of formation are almost the same. Therefore, these stable structures of the Ni-substituted

Table I. Crystallographic data, *viz.* lattice constants and volume, and energy of formation of PdSn₄-based IMCs

Phase	Lattice Constants (Å)	Pd Sites	Volume (Å ³ /atom)	Energy of Formation (kJ/mol atom)
PdSn ₄	$a = 6.55, b = 6.56, c = 11.55$	–	24.794	–26.35
Pd ₃ NiSn ₁₆	$a = 6.49, b = 6.52, c = 11.54$	1	24.392	–22.79
Pd ₃ NiSn ₁₆	$a = 6.49, b = 6.52, c = 11.54$	2	24.392	–22.73
Pd ₃ NiSn ₁₆	$a = 6.49, b = 6.52, c = 11.54$	3	24.393	–23.16
Pd ₃ NiSn ₁₆	$a = 6.49, b = 6.52, c = 11.54$	4	24.393	–22.79
Pd ₂ Ni ₂ Sn ₁₆	$a = 6.39, b = 6.47, c = 11.64$	1 + 2	24.050	–19.79
Pd ₂ Ni ₂ Sn ₁₆	$a = 6.45, b = 6.48, c = 11.52$	1 + 3	24.056	–20.16
Pd ₂ Ni ₂ Sn ₁₆	$a = 6.45, b = 6.47, c = 11.52$	1 + 4	24.053	–20.16
Pd ₂ Ni ₂ Sn ₁₆	$a = 6.45, b = 6.47, c = 11.52$	2 + 3	23.716	–20.20
Pd ₂ Ni ₂ Sn ₁₆	$a = 6.45, b = 6.47, c = 11.52$	2 + 4	24.041	–20.19
Pd ₂ Ni ₂ Sn ₁₆	$a = 6.39, b = 6.46, c = 11.64$	3 + 4	24.041	–19.77
PdNi ₃ Sn ₁₆	$a = 6.39, b = 6.42, c = 11.55$	1 + 2 + 3	23.713	–16.91
PdNi ₃ Sn ₁₆	$a = 6.40, b = 6.43, c = 11.55$	1 + 2 + 4	23.731	–16.91
PdNi ₃ Sn ₁₆	$a = 6.39, b = 6.42, c = 11.55$	2 + 3 + 4	23.716	–16.92
PdNi ₃ Sn ₁₆	$a = 6.39, b = 6.42, c = 11.55$	1 + 3 + 4	23.718	–16.91
NiSn ₄ ²⁰	$a = 6.33, b = 6.35, c = 11.64$	1 + 2+3 + 4	23.381	–13.81
NiSn ₄ ²⁰	$a = 6.34, b = 6.38, c = 11.58$	–	23.433	–12.48
NiSn ₄ ²¹	$a = 6.35, b = 6.37, c = 11.67$	–	23.558	–11.82

phases are subject to further calculations in this work. The results reveal that the calculated energies of formation are all negative with decreasing absolute value as the Ni content is increased, indicating that minor Ni substitution in PdSn₄ will lead to more stable structures. In comparison with pure PdSn₄, the energies of formation of the Ni-substituted phases are higher, indicating that the parent PdSn₄ phase is the most easily formed among the Pd_{1-x}Ni_xSn₄ compounds. For NiSn₄, the lattice parameters and energy of formation are compared with reported *ab initio* values.^{20,21} For convenience, the literature results are summarized in Table I, where the lattice parameters in nanometers in Ghosh's work are converted to angstroms for comparison. The results reveal that the lattice parameters of NiSn₄ calculated herein are similar to previous values with maximum deviation less than 0.52%. For the energy of formation, the maximum absolute difference between this work and the reported results is less than 2 kJ/mol atom, indicating that the calculation method applied herein is reliable and the findings relating to NiSn₄ are trustworthy. Because results for the energy of formation of the other Pd_{1-x}Ni_xSn₄ ($x = 0.25, 0.5, 0.75$) materials have not been reported, the results presented herein cannot be verified either theoretically or experimentally, although this will be a question of time.

Elastic Properties

Pd_{1-x}Ni_xSn₄ compounds, which always appear at the interface between related solders and substrates, serve as an efficient bridging agent for connection. It is known that the stability, stiffness, and anisotropy of materials are closely related to their intrinsic elastic properties. To determine the mechanical stability of the Pd_{1-x}Ni_xSn₄ compounds, the single crystalline elastic modulus is calculated based on the energy change when applying uniform spatial deformation,^{22,23} here in the range from -0.02 to 0.02 in steps of 0.005. For such an orthorhombic crystal system, nine independent elastic matrix elements, viz. C_{ii} ($i = 1 - 6$), C_{12} , C_{13} , and C_{23} , can be derived based on the nine kinds of strain applied to the optimized equilibrium crystal.²⁴ Moreover, the single crystalline elastic constants of the orthorhombic crystal system should obey the following equations:²⁴

$$\begin{aligned} C_{ii} > 0 \quad (i = 1 - 6), \quad C_{11} + C_{22} > 2C_{12}, \\ C_{22} + C_{33} > 2C_{23}, \quad C_{11} + C_{33} > 2C_{13}, \quad (2) \\ C_{11} + C_{22} + C_{33} + 2C_{12} + 2C_{13} + 2C_{23} > 0. \end{aligned}$$

The derived results are listed in Table II. All of the elastic constants calculated for Pd_{1-x}Ni_xSn₄ meet the mechanical stability criteria expressed above. It is obvious that the values of C_{22} are the largest among all the single crystalline elastic

constants of Pd_{1-x}Ni_xSn₄. It is well known that C_{22} represents the incompressibility under uniaxial stress along the crystallographic b -axis. Thus, the resistance of the lattice to deformation is strongest along the b -direction for all of the studied PdSn₄-based intermetallics. The resistance to deformation is related to the atomic bonding character in the considered direction to some extent. To be specific, the bonding character along the b -direction is the largest in contrast to the other directions for all the studied compounds.²⁵ After substitution of Ni at Pd sites in PdSn₄, the values of C_{11} and C_{22} are all prominently increased compared with those for pure PdSn₄, indicating that the resistance to deformation along the a - and b -directions is increased after Ni substitution. However, the values for C_{33} are lower, except for Pd₂Ni₂Sn₁₆, indicating that the resistance to deformation along the c -direction decreases in almost all cases. Considering the structures with different amounts of Ni substitution, note that C_{11} increases up to Pd₂Ni₂Sn₁₆ then decreases for PdNi₃Sn₁₆ then increases again for NiSn₄ with increasing Ni content. Meanwhile, C_{22} increases up to Pd₂Ni₂Sn₁₆ then decreases. For NiSn₄, Ghosh's results for the single crystalline elastic constants are also listed in Table II for comparison with the findings herein. The calculated values are very close to each other, reconfirming the validity of the present model.

The polycrystalline elastic constants of solids, such as the bulk modulus K , shear modulus G , Young's modulus E , and Poisson's ratio ν , are often used to evaluate the resistance of materials to external variation as well as their stiffness and ductile/brittle character. Based on the matrix of single crystalline elastic constants C_{ij} , the polycrystalline elastic character can be derived using the Voigt–Reuss–Hill (VRH) scheme as described everywhere.^{24,26} The hardness H of a material can be obtained from the equation²⁶

$$H = \frac{(1 - 2\nu)E}{6(1 + \nu)}. \quad (3)$$

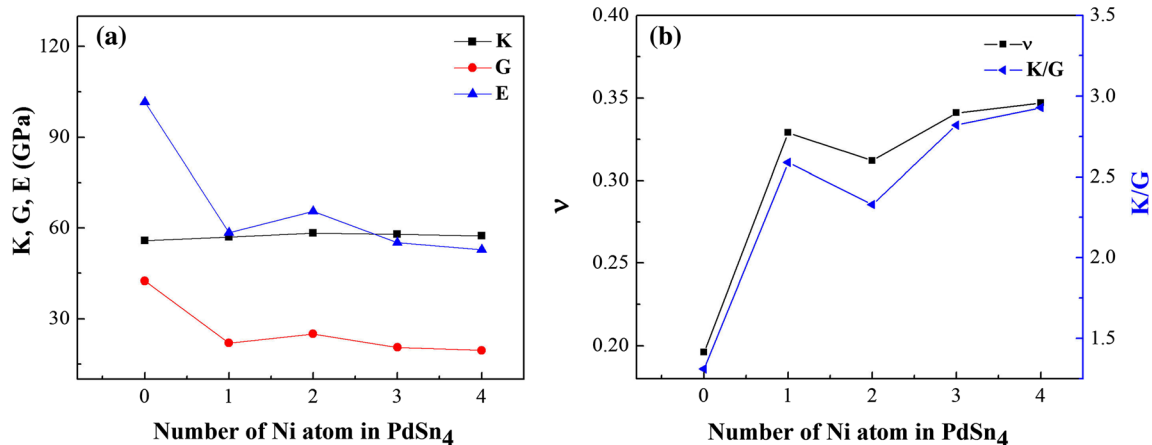
The derived results are all listed in Table III. For NiSn₄, the bulk modulus is 57.36 GPa, which is approximately equal to Ghosh's value of 55.5 GPa with a difference of less than 3.4%, as the single crystalline elastic constants are almost the same. It is found that Ni substitution in PdSn₄ causes a significant decrease of the shear modulus and Young's modulus, while the bulk modulus exhibits a slight increase. The variation trends of the bulk modulus, shear modulus, and Young's modulus with the number of Ni atoms are visualized in Fig. 2a. It is clear that the decreasing tendency in the shear modulus and Young's modulus is not monotonic with increasing Ni content, since Pd₂Ni₂Sn₁₆ exhibits slightly higher values than Pd₃NiSn₁₆. According to the VRH approximation, the shear modulus

Table II. Calculated elastic stiffness (C_{ij} , GPa) of PdSn₄-based IMCs

Phase	C_{11}	C_{22}	C_{33}	C_{44}	C_{55}	C_{66}	C_{12}	C_{13}	C_{23}
PdSn ₄	86.2	99.2	88.1	16.5	13.3	29.0	36.5	40.6	38.0
Pd ₃ NiSn ₁₆	87.9	104.2	85.4	18.3	14.1	29.5	37.2	43.2	38.3
Pd ₂ Ni ₂ Sn ₁₆	94.2	112.9	93.1	17.8	18.1	32.1	36.4	38.2	39.4
PdNi ₃ Sn ₁₆	92.1	107.2	75.5	16.9	13.9	27.2	34.0	45.8	44.1
NiSn ₄	98.1	106.2	67.1	17.5	12.6	25.7	34.4	42.6	47.9
NiSn ₄ ²¹	103.36	113.68	76.96	19.96	13.85	28.72	38.54	36.40	35.74

Table III. Bulk modulus K , shear modulus G , Young's Modulus E , and microhardness H of PdSn₄-based IMCs (units in GPa)

IMCs	K_V	K_R	K	G_V	G_R	G	E	H
PdSn ₄	55.97	55.56	55.77	22.29	20.21	42.50	101.67	8.61
Pd ₃ NiSn ₁₆	57.18	56.82	57.00	22.94	21.03	21.99	58.45	2.51
Pd ₂ Ni ₂ Sn ₁₆	58.68	57.80	58.24	26.01	24.01	25.01	65.63	3.13
PdNi ₃ Sn ₁₆	58.05	57.80	57.93	21.67	19.46	20.56	55.15	2.18
NiSn ₄	57.90	56.82	57.36	20.94	18.26	19.60	52.79	2.00


 Fig. 2. Variation of (a) elastic modulus (unit GPa), and (b) Poisson's ratio ν and K/G ratio (dimensionless) with the number of Ni atoms in PdSn₄.

and bulk modulus for the orthorhombic system are related to the single crystalline elastic constants such as C_{ii} ($i = 1$ to 6) and C_{ij} ($i = 1, 2, 3$). It is found that most of the calculated elastic stiffness constants of Pd₂Ni₂Sn₁₆ are higher than those of Pd₃NiSn₁₆ and PdNi₃Sn₁₆, such as C_{ii} ($i = 1, 2, 3, 5, 6$) as listed in Table II. This causes the higher bulk modulus and shear modulus of Pd₂Ni₂Sn₁₆, leading to its higher Young's modulus. It is known that the bulk modulus denotes the resistance of a material to volume change under pressure and also its resistance to fracture. Meanwhile, the shear modulus is closely related to the resistance of a material to plastic deformation such as shear strain. According to the results presented in Table III, it can be presumed that these materials are not easily compressed after Ni substitution due to their larger resistance to volume change, but they are easily sheared. The Young's modulus is related to the

stiffness of a solid. A larger value of E often corresponds to a stiffer material. It can therefore be deduced that Ni substitution leads to a decrease in the stiffness. This finding is in good agreement with the hardness values H obtained from Eq. (3).

The Poisson's ratio ν and K/G ratio are often used to distinguish ductile from brittle materials.^{27,28} If the Poisson's ratio ν is larger than 0.26, the material will exhibit ductile properties; Otherwise, it will manifest brittle behavior. For K/G , a critical value of 1.75 is usually applied to separate ductile from brittle materials. A value of K/G higher than 1.75 is accompanied by ductility, while a value lower than 1.75 is associated with brittleness. From the results presented in Table IV, the parent PdSn₄ can be classified as a brittle compound. For the Ni-substituted structures, the compounds become ductile and the degree of ductility increases with increasing Ni concentration, except for Pd₂Ni₂Sn₁₆, as shown in

Table IV. Calculated Poisson's ratio ν , K/G ratio, Zener anisotropy factor A_Z , universal anisotropy index A_U , bulk anisotropy index A_K , and shear anisotropy index A_G (all dimensionless)

IMC	ν	K/G	A_Z	A_U	A_K (%)	A_G (%)
PdSn ₄	0.196	1.31	0.66	0.522	0.368	4.894
Pd ₃ NiSn ₁₆	0.329	2.59	0.72	0.460	0.316	4.344
Pd ₂ Ni ₂ Sn ₁₆	0.312	2.33	0.61	0.432	0.755	3.998
PdNi ₃ Sn ₁₆	0.341	2.82	0.58	0.572	0.216	5.373
NiSn ₄	0.347	2.93	0.55	0.753	0.941	6.837

Fig. 2b. Among all the considered compounds, NiSn₄ shows the highest Poisson's ratio and K/G ratio, indicating that the strongest ductile property is obtained if all the Pd atoms are replaced by Ni.

Mechanical Anisotropy

When connecting solders to substrates, microcracks and lattice distortion often appear at the interface because the crystals always manifest different mechanical and thermodynamic properties in different directions. Thus, mechanical anisotropy is an important reference parameter for crystals. The Zener factor can quantitatively index the degree of elastic anisotropic of a crystal. For noncubic crystal systems, it can be derived from single crystalline elastic constants using the expression²⁶

$$A_Z = \frac{2C_{44}}{C_{11} - C_{12}}. \quad (4)$$

If A_Z is equal to 1, the material will be isotropic; Otherwise, it will be anisotropic. A larger departure from unity indicates higher elastic anisotropy. The calculated anisotropy factors are presented in Table IV. According to the calculated values of A_Z , the Pd_{1-x}Ni_xSn₄ compounds are all anisotropic. Among them, NiSn₄ shows the highest degree of elastic anisotropy.

The universal elastic anisotropy index A_U is another evaluation criterion, proposed by Ranganathan et al.²⁹ and expressed as

$$A_U = \frac{K_V}{K_R} + 5\frac{G_V}{G_R} - 6 \geq 0, \quad (5)$$

where K_V , G_V and K_R , G_R are the bulk modulus and shear modulus according to the Voigt and Reuss scheme, respectively. $A_U = 0$ indicates isotropic properties; Otherwise, the properties are anisotropic. Moreover, the greater the value of A_U , the greater the mechanical anisotropy. The calculations reveal that NiSn₄ shows the maximum mechanical anisotropy, while Pd₂Ni₂Sn₁₆ shows the minimum universal mechanical anisotropy. For the parent PdSn₄, the value of A_U falls between that of PdNi₃Sn₁₆ and Pd₃NiSn₁₆ with an intermediate

value of 0.522. Note that, with increasing Ni content in PdSn₄, A_Z first increases then decreases, while A_U first decreases then increases. These different variation trends observed for A_Z and A_U are due to the different methods used to evaluate the anisotropy of the materials, as illustrated above. Although their variation trends are different, the anisotropic nature that they indicate agrees to some degree.

To investigate the degree of elastic anisotropy in compression and shear modes concretely, the dimensionless factors A_K and A_G are calculated respectively using the expressions³⁰

$$A_K = \frac{K_V - K_R}{K_V + K_R}, \quad (6)$$

$$A_G = \frac{G_V - G_R}{G_V + G_R}. \quad (7)$$

According to the results presented in Table IV, NiSn₄ shows the strongest anisotropy of the bulk modulus and shear modulus, with A_K of 0.941% and A_G of 6.837%. Meanwhile, PdNi₃Sn₁₆ and Pd₂Ni₂Sn₁₆ exhibit the lowest anisotropy of the bulk modulus with a value of 0.216% and the lowest anisotropy of the shear modulus with a value of 3.998%, respectively.

To visualize the degree of anisotropy, a three-dimensional (3D) map of the directional Young's modulus can be calculated using the formula³¹

$$\frac{1}{E} = l_1^4 S_{11} + l_2^4 S_{22} + l_3^4 S_{33} + (l_1^2 l_3^2 + l_2^2 l_3^2)(2S_{13} + S_{44}) + l_1^2 l_2^2 (2S_{12} + S_{66}), \quad (8)$$

where l_1 , l_2 , and l_3 are the directional cosines in spherical coordinates about the lattice axes a , b , and c . The S_{ij} are the elements of the inverse matrix of the elastic constants C_{ij} .

A spherical shape of the 3D map always indicates an isotropic crystal, while a large deviation therefrom indicates an anisotropic crystal. The 3D graphical representations of the Young's modulus are shown in Fig. 3, revealing that the Young's modulus of all the PdSn₄-based compounds exhibits prominent anisotropy. Among them, NiSn₄ and PdNi₃Sn₁₆ show an ellipsoidal shape, indicating a more anisotropic Young's modulus than the others, in agreement with the results obtained above for the universal elastic anisotropy index A_U . More details on the anisotropic properties are provided by the projection of the Young's modulus onto the major planes, as shown in Fig. 4. It is found that the shapes projected on the xy plane are all oval. When the Ni fraction is below 5%, the curves projected on the xz planes overlap with those projected on the yz planes and show a flower-like shape. When the Ni fraction is 10%, overlap is observed for the

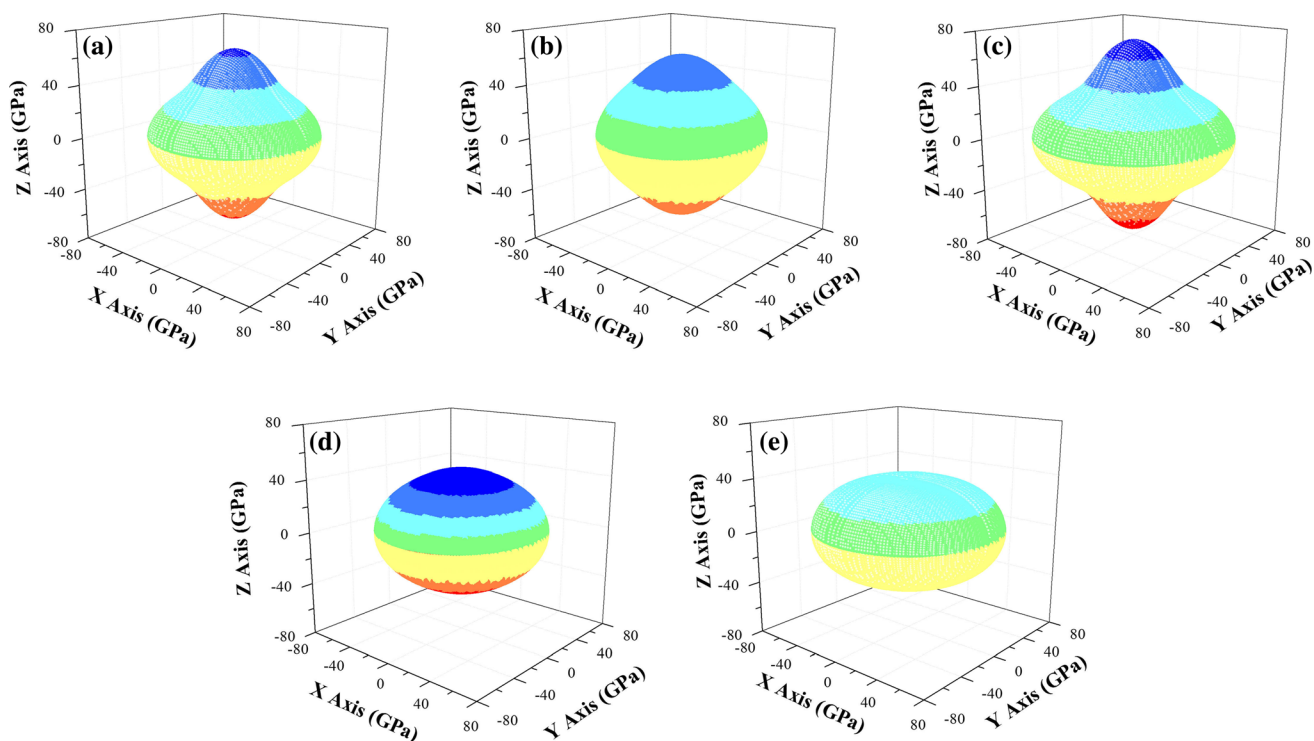


Fig. 3. Direction dependence of Young's modulus (GPa) for PdSn₄-based IMCs: (a) PdSn₄, (b) Pd₃NiSn₁₆, (c) Pd₂Ni₂Sn₁₆, (d) PdNi₃Sn₁₆, and (e) NiSn₄.

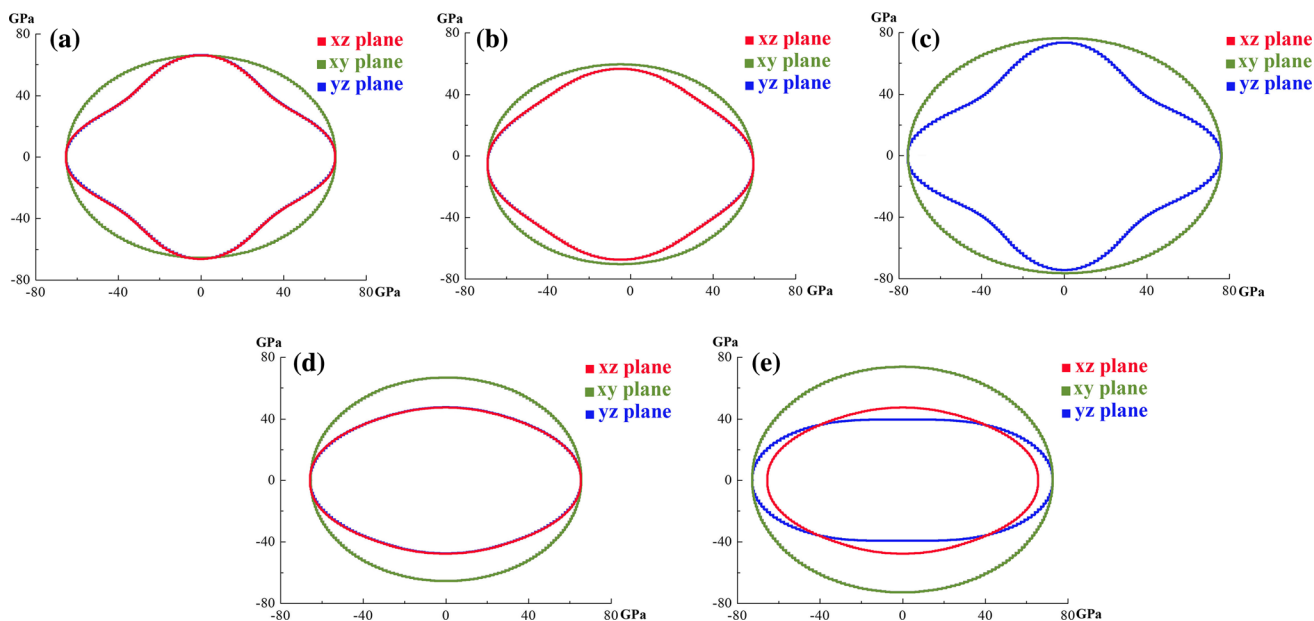


Fig. 4. Projections of directional dependence of Young's modulus (GPa) for PdSn₄-based IMCs: (a) PdSn₄, (b) Pd₃NiSn₁₆, (c) Pd₂Ni₂Sn₁₆, (d) PdNi₃Sn₁₆, and (e) NiSn₄.

projections onto the *xz* and *xy* planes. Above Ni content of 15%, the shapes projected onto the three major planes all become oval. Based on these observations, it can be concluded that fracture will occur most easily along the *xy* plane for lower Ni concentrations below 10%. Beyond that, fracture is more likely to occur on the *yz* plane due to the

higher ratio of major to minor semiaxis, especially for NiSn₄.

Thermodynamic Properties

The intermetallics that form between a solder and substrate play an important role in their connection. To supplement the physical properties of the

Table V. Density ρ (kg/m³), transversal elastic wave velocity v_t , longitudinal elastic wave velocity v_l , average elastic wave velocity v_m (m/s), Debye temperature θ_D (K), and minimum thermal conductivity k_{\min} (W/m-K) at zero temperature and zero pressure for PdSn₄-based IMCs

IMC	ρ	v_t	v_l	v_m	θ_D	k_{\min}
PdSn ₄	7788.45	2325.98	3799.52	2577.82	263.36	0.510
Pd ₃ NiSn ₁₆	7754.04	1684.03	3336.50	1888.10	193.95	0.392
Pd ₂ Ni ₂ Sn ₁₆	7698.90	1802.36	3449.07	2016.33	208.09	0.421
PdNi ₃ Sn ₁₆	7641.21	1640.33	3341.98	1842.10	191.01	0.391
NiSn ₄	7581.21	1607.90	3318.61	1806.97	188.26	0.387

intermetallics described above, their thermodynamic features are now considered in detail. The Debye temperature is widely used to estimate the heat transfer ability of a material at lower temperature; It can be derived from the elastic wave velocity based on the bulk modulus and shear modulus. The equations are not presented herein as they are widely available in published articles.^{26,30} In the present work, the values of the Debye temperature together with the intermediate results for the density, transversal elastic wave velocity v_t , longitudinal elastic wave velocity v_l , and average wave velocity v_m are presented in Table V. Notably, the Debye temperature presents a decreasing tendency with increasing substitution of Ni for Pd in PdSn₄, indicating that substitution degrades the heat transfer ability. Among these materials, Pd₂Ni₂Sn₁₆ exhibits a higher value than the other Ni-substituted intermetallics due to its higher elastic wave velocity.

According to literature, the heat transfer ability decreases at high temperature. To clarify the lower limit of the thermal conductivity at high temperature, Clark's model is used, expressed by the equation³²

$$k_{\min} = 0.87k_B M_a^{-\frac{2}{3}} E^{\frac{1}{3}} \rho^{\frac{1}{6}}, \quad (9)$$

where k_B is Boltzmann's constant, M_a is the average mass per atom, E is the Young's modulus, and ρ is the material's density. The calculated values of k_{\min} are also presented in Table V. It can be seen that substitution of Ni for Pd causes a decrease in the minimum thermal conductivity. The variation trend is in agreement with that found for the Debye temperature. Thus, it can be concluded that Ni substitution degrades the thermal conductivity of PdSn₄. However, the decreasing tendency is not monotonic with increasing Ni concentration, since the minimum thermal conductivity of Pd₂Ni₂Sn₁₆ is slightly higher than the values for the other materials.

Electronic Structure

It is known that the electronic structure has a great impact on the physical properties as well as energy characteristics of materials. To explore this

in greater detail, the total density of states (TDOS) and partial density of states (PDOS) for the PdSn₄-based intermetallics are calculated and shown in Fig. 5. The Fermi level (E_F) is set to zero energy in the TDOS and PDOS. Ni-*d*, Pd-*d*, Sn-*s*, and Sn-*p* electrons are the main contributors to the TDOS of the considered intermetallics. These results reveal that the density of states is nonzero at the level of E_F , indicating a metallic character of these compounds. For pure PdSn₄, Pd-*d* electrons are strongly hybridized with Sn-*p* electrons in the energy range from about -4.9 eV to -2.8 eV accompanied by a sharp high peak in the total density of states. After Ni substitution, Ni-*d* and Sn-*p* electrons mainly dominate the total density of states from -2.8 eV to the Fermi level. Moreover, their hybridization results in a new peak in the total density of states, which seems to shift to the right and intensify with increasing Ni concentration. Meanwhile, the hybridization between Pd-*d* and Sn-*p* electrons in the energy range from -4.9 eV to -2.8 eV appears to weaken. The properties of a material are closely connected with its electronic structure. In previous research, it was found that the absolute value of the energy of formation increases after Ni substitution. It can be deduced that this change may be caused by hybridization of Ni-*d* and Sn-*p* electrons near the Fermi level. In the lower energy range from about -11.0 eV to -5.0 eV, more Sn-*s* together with a little Sn-*p* electrons are the main contributors to the total density of states for all the PdSn₄-based compounds. However, this seems to be insignificant for the energy of formation.

CONCLUSIONS

Lattice structures obtained by substituting Ni at Pd sites in PdSn₄ are studied using first-principles calculations to determine the influence on the structural, mechanical, thermodynamic, and electronic properties. Altogether, five concentrations with a total of 16 structures are considered due to the high solubility of Ni in PdSn₄. The results can be summarized as follows:

1. Substitution causes a decrease in the lattice constants and cell volume due to the smaller atomic radius of Ni compared with Pd. The most stable structures are determined based on the

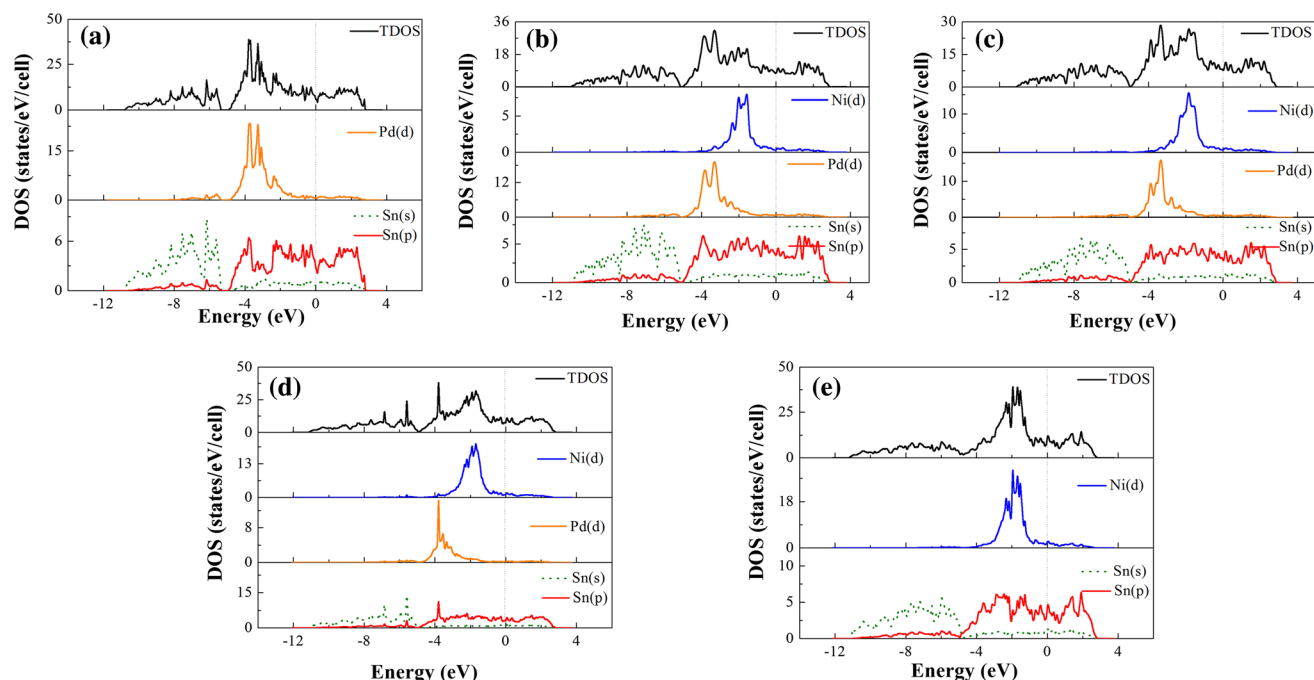


Fig. 5. TDOS and PDOS for PdSn₄-based IMCs: (a) PdSn₄, (b) Pd₃NiSn₁₆, (c) Pd₂Ni₂Sn₁₆, (d) PdNi₃Sn₁₆, and (e) NiSn₄ (dashed lines at 0 eV denote the Fermi level E_F).

energy of formation, revealing that Ni atoms preferentially occupy Pd site 3 for Pd₃NiSn₁₆, sites 2 + 3 for Ni₂Pd₂Sn₁₆ and sites 2 + 3 + 4 for Ni₃PdSn₁₆ due to their lower energy of formation.

- All the studied compounds are thermodynamically stable from the point of view of both energy of formation and mechanical stability. However, the stability decreases after substitution due to a higher energy of formation.
- The resistance of the lattice to deformation is stronger along the *b*-direction than the other directions due to the larger C_{22} value. Substitution results in an increase in the resistance to deformation along the *a*- and *b*-directions.
- The polycrystalline elastic modulus is calculated using the elastic constants C_{ij} . The bulk modulus, Poisson's ratio, and K/G ratio increase while the shear modulus, Young's modulus, and hardness decrease after substitution. There is a change in the properties between the PdSn₄ and Ni-substituted structures. Substitution results in an increase in the ductility of the PdSn₄-based intermetallics. However, PdSn₄ is brittle, while all the Ni-substituted structures are ductile. Among them, NiSn₄ exhibits the highest degree of ductility, while Pd₂Ni₂Sn₁₆ alone behaves differently due to its lower ductility than Pd₃NiSn₁₆.
- The anisotropic property is calculated using the Zener factor A_Z , universal elastic anisotropy index A_U , bulk anisotropy index A_K , and shear anisotropy index A_G . All the compounds show anisotropic properties, which can be visualized

using the 3D surfaces of the Young's modulus and their projections along the major planes. For Ni concentrations below 10%, fracture occurs easily on the *xy* plane, whereas beyond that, fracture is more likely to occur on the *yz* plane.

- According to the Debye temperature and Clark's model, the heat transfer property decreases after substitution.
- The density of states indicates that all the compounds are metallic. Ni substitution decreases the hybridization between Pd-*d* and Sn-*p* electrons in the lower energy range but increases the hybridization of Ni-*d* and Sn-*p* electrons near the Fermi level. This may explain the higher energy of formation of the Ni-substituted phases.

The results of some of the calculations presented herein are compared with available literature values, revealing good consistency. However, some of the results cannot be compared due to the lack of reported experimental or theoretical values. Therefore, these findings should serve as a good reference to predict the properties of such PdSn₄-based intermetallics for verification in future work.

ACKNOWLEDGMENTS

This work was supported by the National Natural Science Foundation of China (51572190); the supercomputing resources were supported by the High Performance Computing Center of Tianjin University, China. The authors would like to

acknowledge Lifang Zhang (Tianjin University of Commerce) and Ping Wu (Tianjin University) for assistance with data analysis and computational work.

REFERENCES

1. C.E. Ho, Y.C. Lin, and S.J. Wang, *Thin Solid Films* 544, 551 (2013).
2. C.E. Ho, W.H. Wu, L.H. Hsu, and C.S. Lin, *J. Electron. Mater.* 41, 11 (2012).
3. J.W. Yoon, B.I. Noh, and J.H. Yoon, *J. Alloys Compd* 509, 153 (2011).
4. S.P. Peng, W.H. Wu, C.E. Ho, and Y.M. Huang, *J. Alloys Compd* 493, 431 (2010).
5. C.-H. Wang, K.-T. Li, and C.-Y. Lin, *Intermetallics* 67, 102 (2015).
6. C.-H. Wang and K.-T. Li, *J. Alloys Compd.* 654, 546 (2016).
7. M.A. Rahman, C.E. Ho, W. Gierlotka, and J.C. Kuo, *J. Electron. Mater.* 43, 4582 (2014).
8. C.-E. Ho, S.-W. Lin, and Y.-C. Lin, *J. Alloys Compd.* 509, 7749 (2011).
9. K. Masui and M. Kajihara, *J. Alloys Compd.* 485, 144 (2009).
10. R. Kubiak and M. Wolcyz, *J. Less-Common Metals* 97, 265 (1984).
11. S.A. Belyakov and C.M. Gourlay, *Intermetallics* 25, 48 (2012).
12. C. Schimpf, P. Kalanke, S.L. Shang, Z.K. Liu, and A. Leineweber, *Mater. Des.* 109, 324 (2016).
13. W.J. Boettinger, M.D. Vaudin, M.E. Williams, L.A. Bendersky, and W.R. Wagner, *J. Electron. Mater.* 32, 511 (2003).
14. G. Kresse and J. Furthmüller, *Phys. Rev. B* 54, 11169 (1996).
15. J.P. Perdew, K. Burke, and M. Ernzerhof, *Phys. Rev. Lett.* 77, 3865 (1996).
16. H.J. Monkhorst and J.D. Pack, *Phys. Rev. B* 13, 5188 (1976).
17. M. Methfessel and A.T. Paxton, *Phys. Rev. B* 40, 3616 (1989).
18. Y. Yang, Y.Z. Li, H. Lu, C. Yu, and J.M. Chen, *Comput. Mater. Sci.* 65, 490 (2012).
19. J. Nylén, F.J. Garcia Garcia, B.D. Mosel, R. Pöttgen, and U. Häussermann, *Solid State Sci.* 6, 147 (2004).
20. S. Ramos de Debiaggi, C. Deluque Toro, G.F. Cabeza, A. Fernández Guillermet, *J. Alloys Compd.* 576, 302 (2013).
21. G. Ghosh, *Metall. Mater. Trans. A* 40A, 4 (2009).
22. S.Q. Wang and H.Q. Ye, *J. Phys.: Condens. Matter.* 15, 5307 (2003).
23. L. Fast, J.M. Wills, B. Johansson, and O. Eriksson, *Phys. Rev. B* 51, 17431 (1995).
24. J.L. Du, B. Wen, R. Melnik, and Y. Kawazoe, *J. Alloys Compd.* 588, 96 (2014).
25. M.L. Wang, Z. Chen, C.J. Xia, Y. Wu, and D. Chen, *Mater. Chem. Phys.* 197, 145 (2017).
26. H.-C. Cheng, C.-F. Yu, and W.-H. Chen, *J. Alloys Compd.* 546, 286 (2013).
27. X.D. Zhang, C.H. Ying, and Z.J. Li, *Superlattices Microstruct.* 52, 459 (2012).
28. C.M. Li, S.M. Zeng, and Z.Q. Chen, *Comput. Mater. Sci.* 93, 210 (2014).
29. S.I. Ranganathan and M. Ostojica-Starzewski, *Phys. Rev. Lett.* 101, 055504 (2008).
30. Y. Liu, X. Chong, Y. Jiang, R. Zhou, and J. Peng, *Phys. B Condens. Matter* 506, 1 (2017).
31. Y.H. Duan, Y. Sun, and M.J. Peng, *Comput. Mater. Sci.* 92, 258 (2014).
32. D.R. Clarke and C.G. Levi, *Annu. Rev. Mater. Res.* 33, 383 (2003).

Publisher's Note Springer Nature remains neutral with regard to jurisdictional claims in published maps and institutional affiliations.